Journal of Power Sources 211 (2012) 77–83

Contents lists available at SciVerse ScienceDirect

Journal of Power Sources

journal homepage: www.elsevier.com/locate/jpowsour

A novel method to determine the particle–particle fracture of yttria stabilized zirconia

Yunlong Wang, Yanxiang Zhang, Changrong Xia*

CAS Key Laboratory of Materials for Energy Conversion, Department of Materials Science and Engineering, University of Science and Technology of China, Hefei 230026, Anhui, China

ARTICLE INFO

Article history:
Received 9 December 2011
Received in revised form
20 March 2012
Accepted 21 March 2012
Available online 10 April 2012

Keywords:
Yttria stabilized zirconia
Conductivity
Composites electrode
Thermal expansion
Particle–particle fracture

ABSTRACT

A novel method is presented to determine the particle–particle fracture of yttria stabilized zirconia (YSZ), which is crucial in predicting the thermal cycle properties of solid oxide fuel cells (SOFCs). The method is demonstrated by determining the Weibull and normal distribution parameters via resistivity variation of YSZ–Al_2O_3 composites undergoing thermal cycle processes. A straightforward approach is developed to relate YSZ mechanical property with its conductivity based on fracture statistics distributions and percolation theory. By the measurement of the conductivity change in thermal cycles, the fracture between YSZ particles caused by thermal stress can be statistically "counted", approaching these parameters with a statistical principle, and offering a possible way to understand particle–particle fracture in microscale, and to predict the effect of microstructure change using electric signals. Finally, this method offers a potential to precisely forecast the performance degradation in the different thermal cycle processes for SOFC components such as doped ceria electrolytes and perovskite electrodes.

1. Introduction

Solid oxide fuel cells (SOFCs) are a forward looking technology for highly efficient, environmental friendly power generation [1–3]. Nevertheless, they have a common requirement for high durability in thermal cycling due to the fault condition or maintenance shutdown. Therefore, thermal cycling durability is a desirable feature for SOFC commercial applications [4]. There have been many observations documented about the effects of thermal cycling on SOFCs. Bujalski et al. [5] have studied the transient performance of SOFCs under various thermal cycling conditions to understand the degradation mechanisms. Taniguchi et al. [6] have reported cracks formation in electrolyte-supported planar SOFC undergoing only one thermal cycle. Despite the effect of temperature gradients, the performance degradation in thermal cycling is essentially a mechanical process, induced by the mismatch of coefficients of thermal expansion (CTE) between the fuel cell materials. Since the real failure is difficult to be measured and/or observed during thermal cycling in experiments, thermo-mechanical models are developed to calculate the residual stresses at room temperature [7,8] and thermal stresses at the operating conditions [9] in SOFCs using finite element-based approach. Combining with the Weibull analysis [8,10] and/or a multi-scale micromechanics model [11], the thermal cycling durability can be predicted base on the mechanical properties of the relevant components of solid oxide fuel cells.

However, for thermo-mechanical models, much attention is paid for the structural integrity in a relatively large scale, and few researches have been conducted to the failure inside the composite electrodes, which are widely used to extend the reaction sites. There is always difference in the thermal expansion coefficients of composite components. In typical composites such as $(La_{0.85}Sr_{0.15})_{0.9}MnO_{3-\delta}$ (LSM)–$(Y_2O_3)_{0.08}(ZrO_2)_{0.92}$ electrodes, the difference is relatively small. However, the difference can be very large in some composites such as $La_{0.6}Sr_{0.4}CoO_{3-\delta}$–$Sm_{0.2}Ce_{0.8}O_{1.9}$. The different thermal expansion behavior builds up thermal stress which will cause cracking in thermal treatments, typically thermal cycle. Due to the high porosity of the electrode, cracking will suspend in pores and the failure presents particle–particle fracture. The particle–particle fracture caused by the thermal stress not only blocks the electronic and oxygen ions transportation, but also destroys the so-called three-phase boundaries (TPBs), which are critical for electrode performance. Consequently, the electrochemical performance degrades and the interfacial polarization resistance increases [12]. Therefore, for practical applications, it is crucial to understand the evolution of the particle–particle fracture so as to evaluate the electrochemical properties as well as the structural reliability regarding thermal treatments such as heating,

* Corresponding author. Tel.: +86 551 3607475; fax: +86 551 3601592.
E-mail address: xiacr@ustc.edu.cn (C. Xia).

0378-7753/$ – see front matter © 2012 Elsevier B.V. All rights reserved.
doi:10.1016/j.jpowsour.2012.03.063

thermal cycle. However, the particle–particle failure characteristics such as the parameters for the Weibull distribution of SOFC components are still difficult to find in literatures, due to the difficulty in manufacturing or testing [13].

In this work, a novel method is presented to determine the particle–particle fracture of typical SOFC component, yttria stabilized zirconia (YSZ). Fracture is described by monitoring the gradual decrease in conductivity (or increase in resistivity) of the conductive ceramic composites (YSZ–Al_2O_3) undergoing heating and cooling processes. The conductivity change is linked quantitatively with percolation theory to fracture evolution within the composites. In general, conductivity is directly bound up with the coordination number of the conductive component in a porous composite consisting of a conductive and an insulative material [14,15]. When a tensile stress is applied to the conductive phase, the coordination number decreases as a result of particle–particle fracture, thus increasing the resistivity. The increment therefore presents the statistic fracture between the conductive particles. In other words, the probability of failure between the conductive particles may be counted via the increment based on percolation theory which is a well developed statistic principle regarding the conductivity and particle connection of composite systems. Furthermore, the temperature change is related quantitatively to a stress which is in situ generated due to CTE mismatch and applied directly on the particles undergoing thermal-cycle processes. In another word, various stresses can be applied via the changes of temperature. Accordingly, particle–particle fracture can be quantitatively linked to the stress. Therefore, this method offers potential for understanding the fracture between particles, which are microscale in size and comparable to the fracture inside the electrode at any temperature ranges. Moreover, this method is also applicable to the other SOFC materials such as doped ceria electrolytes and perovskite electrodes.

2. Theoretical development

2.1. Thermal stress applied to the conductive particles

The YSZ–Al_2O_3, which is used to determine the particle–particle failure of YSZ, is a conductive composite that is composed of a conductive phase (YSZ) and an insulative phase (Al_2O_3). The two phase particles are frequently considered as a random packing system as illustrated in Fig. 1a, where *i* represents the conductive phase and *j* the insulative phase. The composite is practically synthesized when the two-phase particles are thoroughly mixed and sintered at high temperature, resulting in strong connection between particles, and thus forming *i* and *j* phase networks as well as pores. The conductive and insulative networks are in stress free state when they are formed by heating the loosely packed particles at the sintering temperature (Fig. 1a). However, stress is generated and applied to each other when the temperature decreases since their CTEs are different. The stress is a function of the CTEs and the average CTE, α_{ave}, which can be estimated as [8,16]

$$\alpha_{ave} = \left(\alpha_i \overline{E}_i + \alpha_j \overline{E}_j\right)/\left(\overline{E}_i + \overline{E}_j\right) \quad (1)$$

where $\alpha_{i(j)}$ and $\overline{E}_{i(j)}$ are the CTE and effective moduli of single *i*(*j*) phase, respectively. The modulus can be simplified as [8,16,17]

$$\overline{E}_i = E_i\phi_i\left(1-\phi_g\right)\Big/(1-2\nu_i) \quad (2a)$$

$$\overline{E}_j = E_j\phi_j\left(1-\phi_g\right)\Big/(1-2\nu_j) \quad (2b)$$

where $E_{i(j)}$ and $\nu_{i(j)}$ are the Young's modulus and the poisson ratio corresponding to fully dense *i*(*j*) phase materials. φ_g is the porosity of the composite. $\varphi_{i(j)}$ is the volume fraction of the conductive (*i*) and insulative (*j*) particles to the total solid material, respectively, $\varphi_i + \varphi_j = 1.00$.

The porous composite can also be considered to consist of *i* phase and *j* phase using the interface and steric hindrance. When the composite experiences a process of cooling from the sintering temperature to a low temperature, stresses are gradually generated and applied to the *i* and *j* phase networks due to the CTE mismatch. The balance strain $\Delta\varepsilon_{balance}$ (Fig. 1b) and the free strain $\Delta\varepsilon_i$ (Fig. 1c) and $\Delta\varepsilon_j$ (Fig. 1d) for *i* and *j* phase network, respectively, are given by [4]

$$\Delta\varepsilon_{balance} = \alpha_{ave}\Delta T \quad (3a)$$

$$\Delta\varepsilon_i = \alpha_i\Delta T \quad (3b)$$

$$\Delta\varepsilon_j = \alpha_j\Delta T \quad (3c)$$

where ΔT is the temperature difference. So, imposition of these different strains between the free and balance state results in

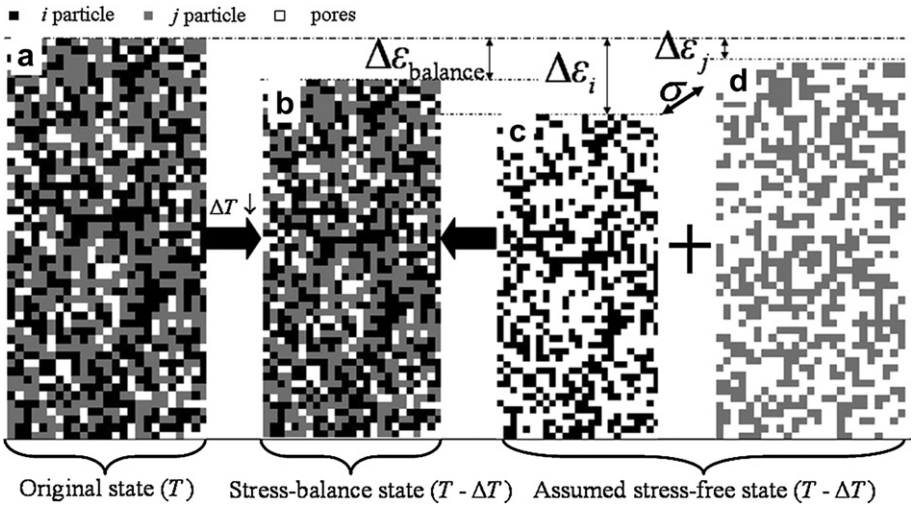

Fig. 1. Schematic diagram of (a) a two-phase porous composite in the original state without any stress; (b) in stress balance state; (c) the network of the single *i*-phase in stress free state; and (d) the network of the single *j*-phase in stress free state, assuming that CTE of *i*-phase (YSZ) is higher than *j*-phase (Al_2O_3).

a couple of equal and opposite stresses, σ_i acts in i phase network and σ_j acts in the j phase network. Holding $\sigma_i = -\sigma_j = \sigma$, so [4]

$$\sigma_i = (\alpha_i \Delta T - \alpha_{ave}\Delta T)\overline{E}_i \quad (4a)$$

$$\sigma_j = (\alpha_j \Delta T - \alpha_{ave}\Delta T)\overline{E}_j \quad (4b)$$

$$\sigma = (\alpha_i - \alpha_j)\Delta T/(1/\overline{E}_i + 1/\overline{E}_j) \quad (4c)$$

Thus, in the cooling process, a tensile stress is generated by the network of the phase with low CTE (j phase in Fig. 1) and applied to the network of the phase with high CTE (i phase in Fig. 1) and of course to the particles. Because the i phase particles are uniformly mixed with the j phase particles to form a composite which is theoretically considered as a random packing system, the expansion of the network can be assumed to be homogeneous and the particles are expected to suffer the same normal stress. This stress is not introduced from outside but in situ generated by the composite itself in the cooling process. It is gradually released when the composite undergoes a heating process. In general, the CTEs depend on temperature. For ceramic materials such as Al_2O_3 and YSZ, CTEs are almost constant in temperature ranges where phase transformation does not happen. In this work, mean CTE values are used to simplify the calculation process. And then, the stress depends linearly with the temperature. Inversely, the stress can be precisely controlled by varying the temperature. For instance, Fig. 2 shows the $\sigma-\Delta T$ relations for LSM–YSZ, LSM–Al_2O_3 and YSZ–Al_2O_3 composites. Their mechanical and thermal properties are summarized in Table 1. In addition to the temperature difference, the thermal stress depends on the mismatch of CTE, and the mechanical properties. High CTE mismatch corresponds to high stress. However, though the CTE mismatch between LSM and Al_2O_3 is larger than that for YSZ and Al_2O_3, the thermal stress in the LSM–Al_2O_3 composite is smaller than that in the YSZ–Al_2O_3 due to the weak mechanical properties of LSM. Clearly, the thermal stress is in situ generated, and can be quantitatively controlled by varying the temperature difference.

2.2. Statistically counting of particle–particle fractures

For a conductive composite as show in Fig. 1a, when the i phase is conductive and the j phase is insulative or the conductivity of j phase is negligible compared with the i phase, according to the percolation theory [13], its resistivity (ρ), which is the reciprocal of the composite conductivity, is given by [14,15,21]

$$\rho = \gamma\rho_0\left[1/(1-\phi_g)\right]^{\zeta}[(1-n_c)/(n_i-n_c)]^{\mu} \quad (5)$$

where μ is a universal exponent, $\mu = 2.00$ in a three dimensional system [15]. ρ_0 is the resistivity of pure i phase material. ζ is the Bruggeman factor that accounts for tortuous conduction pathways, and it is typically assumed to be 1.50 [21]. γ is an adjustable parameter which takes account the effect of the necks between particles and can be experimentally determined. n_i is the fraction number of the conductive particles, and n_c is the critical fraction number or the percolation threshold below which the composite is not conductive. The fraction number can be ascertained with [15]

$$n_i = k^2\Big/\left(k^2 - 1 + \overline{Z}/Z_{i-i}\right) \quad (6a)$$

$$n_c = k^2\Big/\left(k^2 - 1 + \overline{Z}/Z_c\right) \quad (6b)$$

where $k = r_j/r_i$ and r_i, r_j denote the radius of conductive and insulative particles, respectively. $\overline{Z}$ is the average total coordination number in a random packing system of mono-sized spheres, which is widely assumed that $\overline{Z} = 6.00$, [14,15] for a porous randomly packing system, It should be noted $\overline{Z}$ value is different for dense ceramics. Z_c is the coordination number at the percolation threshold and $Z_c = 1.76$ [14,15,22]. Z_{i-i} is the average coordination number among the i phase particles, and is a function of the composition and k as [14,15]

$$Z_{i-i} = \overline{Z}\phi_i\Big/\left(\phi_i + \phi_j/k\right) \quad (7)$$

Combining Eqs. (5, 6a, 6b), it is noted that the resistivity is only a function of the average coordination number among the conductive particles for the same composite, where its composition, porosity and particle sizes are fixed. That is, Z_{i-i} can be experimentally determined by measuring the resistivity.

In the cooling process, the tensile stress could fracture i–i particle connection. The neck is not conductive at all once it is broken by the stress. Accordingly, the conductive coordination number is reduced, i.e. reducing the average coordination number Z_{i-i}. Fig. 3 shows the relation between Z_{i-i} reduction and resistivity increase. The original Z_{i-i} is set to be 4.00 and k is assumed to be 0.641. For instance, when 1.00%, 5.00% and 10.0% i–i connection is fractured, ρ increases 5.00%, 28.5% and 68.1% for an Al_2O_3–YSZ composite, respectively. Therefore, the particle–particle fracture ratio could be determined by measuring the resistivity. Since the composite resistivity is calculated based on the percolation theory, which is derived with probability statistics method, the fracture is thus statistically counted in the present method. In the following heating process, the stress is released gradually and the cracking could hardly be recovered for brittle materials when the temperature is much lower than the sintering temperature. Practically, the applied temperature of a ceramic composite is usually much lower than its fabrication temperature. For example, LSM–YSZ composite electrodes are sintered at 1100–1200 °C while they are operated at

Table 1
The properties of $(La_{0.85}Sr_{0.15})_{0.9}MnO_{3-\delta}$ (LSM), $(Y_2O_3)_{0.08}(ZrO_2)_{0.92}$ (YSZ) and Al_2O_3.

Material	Density (g cm^{-3})	Young's modulus (GPa)	Poisson ratio	CTE ($\times 10^{-6}$ °C^{-1})	Refs.
LSM	–	29.7	0.300	11.7	[16]
YSZ	5.99	212	0.320	10.0	[18,19]
Al_2O_3	3.90	380	0.250	8.00	[20]

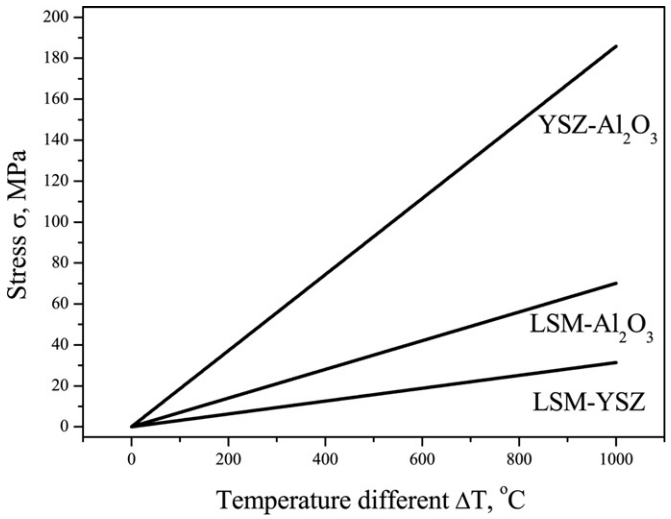

Fig. 2. Thermal stress at various temperature difference for YSZ–Al_2O_3, LSM–Al_2O_3 and YSZ–LSM porous composites ($\varphi_i = \varphi_j = 0.500$ and $\varphi_g = 0.440$).

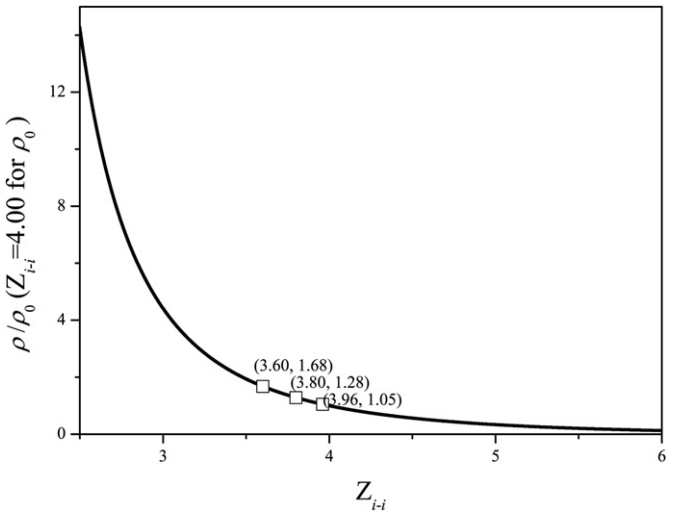

Fig. 3. Resistivity change ρ/ρ_0 versus coordination number between conductive particles Z_{i-i} for YSZ–Al_2O_3 composites ($k = 0.641$ and $Z_{i-i} = 4.00$ for ρ_0).

about 800 °C. So, the *i*–*i* connection could be broken in the cooling process while the disconnected particle neighbors could not be re-connected in the following heating process. That is, in each thermal cycle process, the coordination number decreases. When only a few thermal cycles are conducted and the probability of particle–particle failure is very small, the mechanical properties of each phase network can be assumed to be invariable. That is, the probability of failure is independent of the previous loading, after *N* heating–cooling cycles, the coordination number is

$$Z_{i-i,N} = Z_{i-i}\left(1 - P_f\right)^N \tag{8a}$$

where $Z_{i-i,N}$ is the average coordination number after *N* thermal cycles, and P_f is the probability of particle–particle failure. Eqs. (5)–(8) and Fig. 3 demonstrate that the probability of failure, P_f, is experimentally determinable, inferring that the method is a bridge from electric signals to the cracking in the materials.

3. Experimental procedure

The method was validated with ceramic composites consisting YSZ (8% mole yttria stabilized zirconia) and Al_2O_3. YSZ is an oxygen ionic conductor while Al_2O_3 is an insulator. To prepare the composites, YSZ (Jiujiang Fanmeiya Advanced Materials Co., Ltd., China) and Al_2O_3 (Tianjin Guangfu Fine Chemical Research Institute, China) powders were mixed with ethanol, ball-milled for 2 h, and dried at 120 °C. The dried mixture was then cold-pressed under 120 MPa to form green pellets. The weight ratios of YSZ to Al_2O_3 were 100:0 (pure YSZ), 85:15, 80:20 and 75:25 in the composites. The green samples were subsequently sintered at 1100 °C for 2 h, resulting in YSZ–Al_2O_3 composites about 15 mm in diameter and 0.7 mm thick. 1100 °C is a typical sintering temperature for SOFC cathodes such as YSZ–LSM composites. Three parallel samples were fabricated and tested for each composition. Density was measured using the Archimedes method. Ag paste and Ag wires were used for current collection. The samples were heated at 0.050 °C s^{-1} to the test temperature, where they were stabilized for 600 s to measure the impedance spectrum using an electrochemical station (IM6e, ZAHNER) with a frequency range from 0.01 Hz to 100 kHz and a 10.0 mV perturbation. The resulting curve is known as Nyquist-plot from which the resistance can be derived. The samples were then slowly cooled at 0.050 °C s^{-1} to the next testing temperature. Thermal cycles were also performed at heating and cooling rate of 0.050 °C s^{-1}. The microstructure and morphology of the samples were characterized using scanning electron microscopy (SEM, FEI XL30).

4. Results and discussions

4.1. Resistivities of dense and porous YSZ samples

YSZ is an oxygen ionic conductor. Its resistivity is often measured using impedance spectroscopy. Fig. 4 shows the typical Nyquist-plots recorded at 800 °C on dense and porous YSZ samples. The high frequency intercept with the real axis corresponds to the ohmic resistance. The dense YSZ pellet, which is prepared by sintering the 100:0 (pure YSZ without any Al_2O_3) sample at 1500 °C for 5 h, exhibits a resistivity of 28.0 Ω cm, the value agrees well with the literature data [23]. Therefore, ρ_0 is determined to be 28.0 Ω cm in Eq. (5). The porous YSZ, which is obtained by sintering the green sample at 1100 °C for 2 h, shows a resistivity of 122 Ω cm. The porous sample has a high resistivity as expected from Eq. (5). Its porosity φ_g is 0.410. The pores block the transport of the oxygen ionic species and make the transportation path tortuous. Consequently, the resistivity becomes bigger at higher porosity. Furthermore, because of the low sintering temperature, the contact

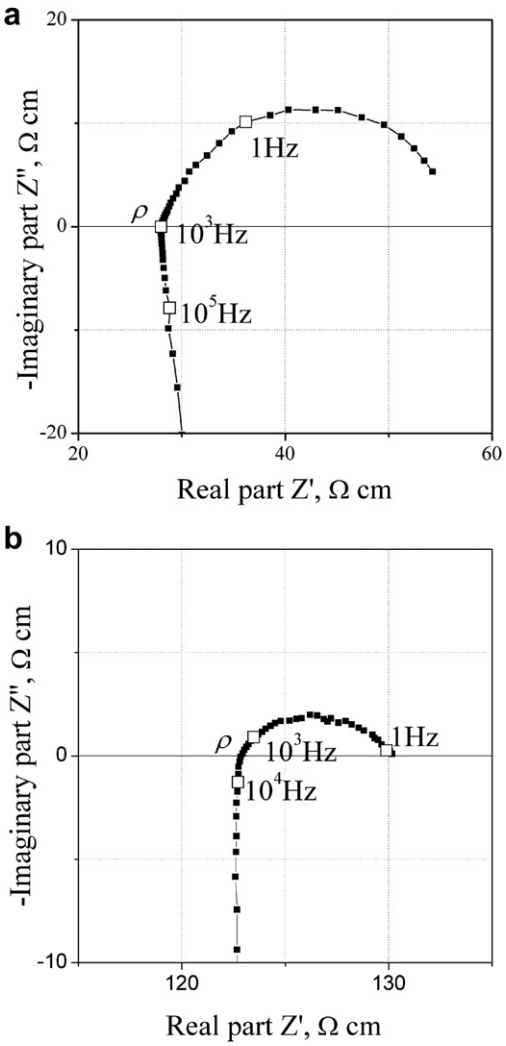

Fig. 4. Typical Nyquist-plots measured at 800 °C for (a) dense YSZ; and (b) porous YSZ. The high frequency intercept with the real axis corresponds to the ohmic resistance of the YSZ sample.

area between particles is small, i.e. the sintered neck is weak. Thus the boundary resistance increases. Combining the resistivities of the dense and porous YSZ samples, the adjustable parameter γ, which takes account the effect of the necks between particles, is calculated to be 1.98 using Eq. (5). Under fixed sintering conditions, the sintering necks between particles are almost identical for various samples, and thus γ is a constant.

4.2. Resistivities of porous YSZ–Al_2O_3 composites

For the YSZ–Al_2O_3 composites with different compositions, Eqs. (5)–(7) demonstrate that the resistivity is a function of coordination number, which depends on the composition. Fig. 5 shows the resistivity of YSZ–Al_2O_3 composites with different composition. With the increasing of the Al_2O_3 content, more and more position of YSZ is substituted by Al_2O_3, the average coordination number between conductive particles decreases, and thus the resistivity increases. The specific value can be calculated using the percolation theory combining with the porosity, which is about 0.440 for all the composites sintered at 1100 °C for 2 h. By fitting the experiment data using Eqs. (5)–(7), the effective size ratio, k, can be determined, $k = 0.641$. When the porosity and size ratio is experimentally determined, the resistivity is only a function of the composition. The predicted resistivity is also shown in Fig. 5. The estimated line agrees very well with the experiment, demonstrating that the percolation model is a well developed theory in predicting composite resistivity, further clarifying that the resistivity is a function of coordination number which depends only on the composition and microstructures such as porosity and particle size. That is to say, by evaluating the electric resistivity change, the evolution of the coordination number between conductive particles can be exactly obtained. The coordination number is derived and shown also in Fig. 5 as the upper x-axis to further demonstrate the dependence of resistivity on the coordination number.

4.3. Resistivity evolution and particle–particle fracture in thermal cycle processes

For pure YSZ samples, Fig. 6a shows that the resistivity keeps xalmost constant in thermal cycle processes. The unchanged resistivity demonstrates that the conductive coordinate number

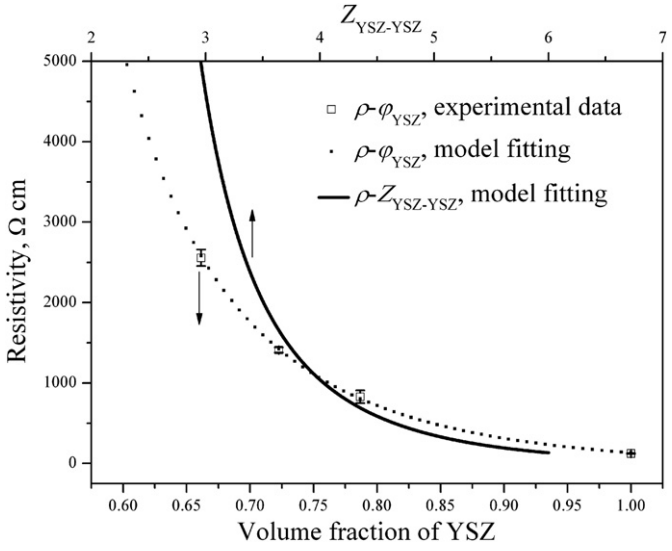

Fig. 5. Resistivity at 800 °C as a function of YSZ content and average coordination number between YSZ–YSZ particles for YSZ–Al_2O_3 composites. The coordination number is derived with Eq. (7) from the content.

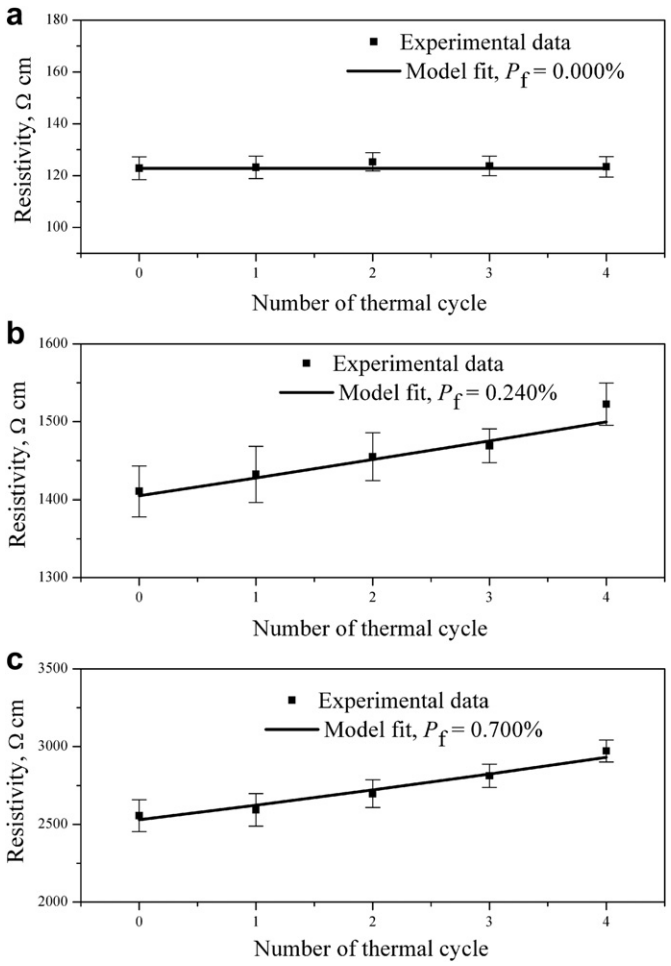

Fig. 6. Resistivity at 800 °C of YSZ–Al_2O_3 composites undergoing RT-800 °C thermal cycle processes (a) pure YSZ; (b) YSZ: Al_2O_3 = 80:20 (wt.); (c) YSZ: Al_2O_3 = 75:25 (wt.).

remains the same. This result further exhibits that the contact between YSZ particles is not damaged in the RT-800 °C thermal cycle processes. Therefore, no tensile stress or negligible stress is generated and applied to the YSZ networks. Actually, a failure probability of 0.000% is derived. This suggests that temperature gradient in the samples is negligible when the heating and cooling are conducted at 3 °C min^{-1}. So, for the composite samples, the resistivity changes are caused only by the thermal stress that originates only from the CTE mismatching of YSZ and Al_2O_3. At the sintering temperature of 1100 °C, the composite is in stress free state, i.e. $\sigma = 0$. When the temperature drop to 800 °C, assuming the thermal stress is σ_0, and the sample is in its original state. Fig. 6b shows the resistivity change of YSZ–Al_2O_3 composites containing 20.0 wt.% Al_2O_3. The failure probability of the connection between YSZ particles is estimated to be 0.240% using Eqs. (5)–(8a). For composites with more Al_2O_3, failure gets easier due to higher stress as suggested with Eqs. (2a, 2b, 4c). As shown in Fig. 6c, the failure probability increases to 0.700% for the composites with 25.0 wt.% Al_2O_3. The thermal cycle process is not further performed because the Al_2O_3 networks may also suffer slight destruction, which might change their mechanical properties. It should be note that the model fitting lines shown in Fig. 6 are almost linear, because the failure probability is so small (less than 1.000%) that Z_{i-i} changes almost linearly with N according to Eq. (8a), That is:

$$Z_{i-i,N} = Z_{i-i}\left(1 - NP_f\right) \tag{8b}$$

Moreover, the overall decrease of Z_{i-i} is small too (less than 3.00%). In this case, there is a good linear relationship between the resistivity and Z_{i-i} when the change of Z_{i-i} is in a very narrow range as shown in Fig. 3. Therefore, the resistivity changes almost linearly via the number of thermal cycles as shown in Fig. 6.

Fig. 7a shows the cross-sectional images of the composite with 25.0 wt.% Al_2O_3. YSZ particles are bigger than Al_2O_3 particles. Both particles are not monodistributed. So, the specific size ratio can not be obtained from the micrographs. But the effective ratio of the particle radius k can be estimated by fitting the resistivity data. There are no obvious cracking in the original sample. However, the networks suffer a partial destruction as show in Fig. 7b due to the particle–particle fractures after four thermal cycles. Because of the high porosity (0.440), the fracture vanishes when the cracking spreads to the edge of the pores. And each fracture is almost independently. That is, the particle–particle fracture does not affect the stress state of their neighboring particles. The micro-crack shown in Fig. 7b is the result of the independently particle–particle fracture linking.

4.4. Particle–particle fracture of YSZ

The strength of a brittle material is not a well defined quantity and has to be described with respect to fracture statistics. As it is well known, the Weibull distribution with a flexible two-parameter analytic formula has been found to successfully describe a large body of fracture data for brittle materials [24]. It describes the relationship between the probability of failure, P_f, of a perfectly elastic body under a tensile stress, σ. The simplified Weibull equation [10,24], which is widely used in estimating the chance of failure of ceramics, given by

$$P_f(\sigma) = 1 - \exp\left[-(\sigma/\Sigma)^m\right] \tag{9a}$$

where $\sum$ is a normalized material strength (scale parameter) and m the Weibull modulus (shape parameter). Then, the probability density function of the Weibull distribution $p_f(\sigma) = dP_f(\sigma)/d\sigma$ is given by

$$p_f(\sigma) = m\left(\sigma/\sum\right)^{m-1}\exp\left[-(\sigma/\Sigma)^m\right]/\sum \tag{9b}$$

However, the Weibull distribution should be considered as an empirical one on an equal footing with other distribution functions like normal distribution which is natural one to apply to the brittle materials manufactured and handled without special care. Its probability density function [25] is

$$p_f(\sigma) = \frac{1}{\sqrt{2\pi}\delta}\exp\left\{-\left[(\sigma-\overline{\sigma})^2/2\delta^2\right]\right\} \tag{9c}$$

Where $\overline{\sigma}$ and δ are the mean and standard deviation, respectively.

For each distribution, the parameters can describe fracture strength meticulously. By determining the parameters using the particle–particle fracture probability at various tensile stresses associated with the temperature different. The fracture between particles can be quantitatively characterized. Accordingly, the performance attenuation can be predicted regarding conductivity and residual intensity degradation caused by cracking in thermal treating processes.

For composites with different composition, the stress can be calculated with Eqs. (2)–(4), and the failure probability under the stress can derive from the resistivity. So, the Weibull parameters are derivable with Eq. (9a). The results are $\sum = 290$ MPa and $m = 11.4$. For the normal distribution, $\overline{\sigma} = 302$ MPa and $\delta = 46.5$. These parameters indicate the probability of failure between particles under a tensile stress, Fig. 8a. Under low tensile stress range (<220 MPa), the results for different distribution are similar. Thus, this work provides a novel method to approach the values of the parameters and understand the fracture in a small scale.

4.5. Resistivity prediction in various thermal cycle processes

The σ–P_f distribution shown in Fig. 8a is widely used in failure prediction where σ is directly applied to the objective material. However, it is an indirect forecast for a free-standing composite undergoing thermal cycle process since σ is not directly applied but in situ generated due to CTE mismatch. In the thermal treating processes, the controllable parameter is temperature. In case the temperature gradient within the composite is negligible when the cooling and heating rates are relatively low (Fig. 6a), σ has a linear relation with ΔT (Fig. 2), the difference between the upper temperature (T_h) and bottom temperature (T_l) of the thermal cycle range. Therefore, Fig. 8a can be converted to Fig. 8b, in which P_f is plotted as a function of $\Delta T = T_h - T_l$ for an YSZ–Al_2O_3 composite containing 25.0 wt.% Al_2O_3. The ΔT–P_f curve should be much more convenient for practical applications where the conductive composites have to endure thermal cycles in different temperature ranges. An experiment is designed to verify the model prediction. Fig. 8c shows the resistance evolution with time and ΔT. The resistance is measured at 800 °C. It increases with cycle number

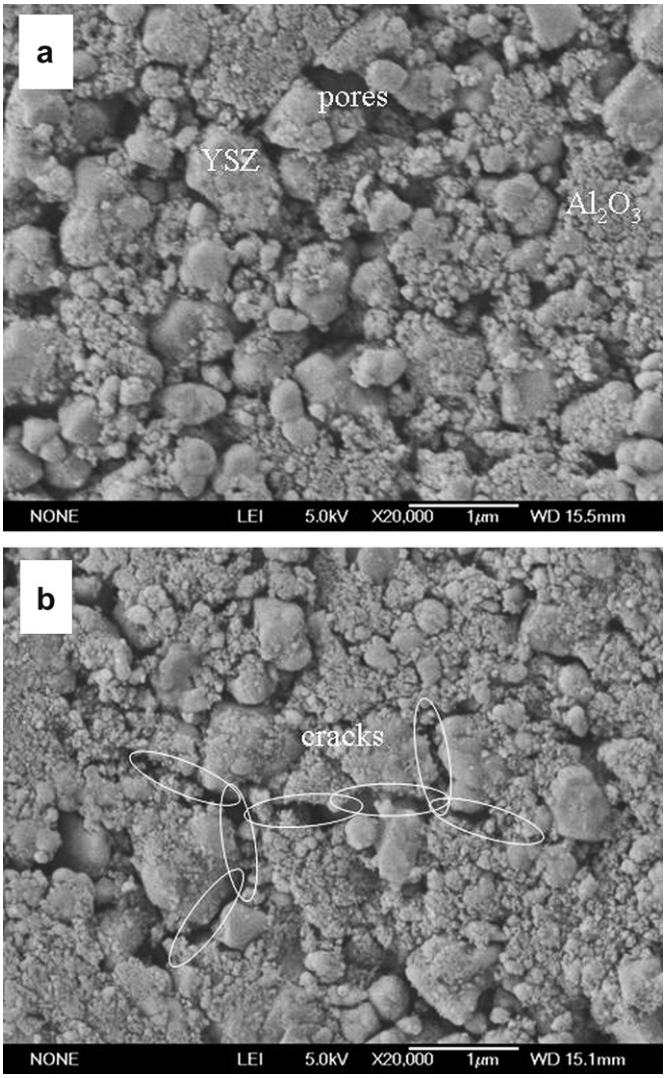

Fig. 7. Cross-sectional images of the composite with 25 wt.% Al_2O_3 (a) in the original state and (b) after four RT-800 °C cycles.

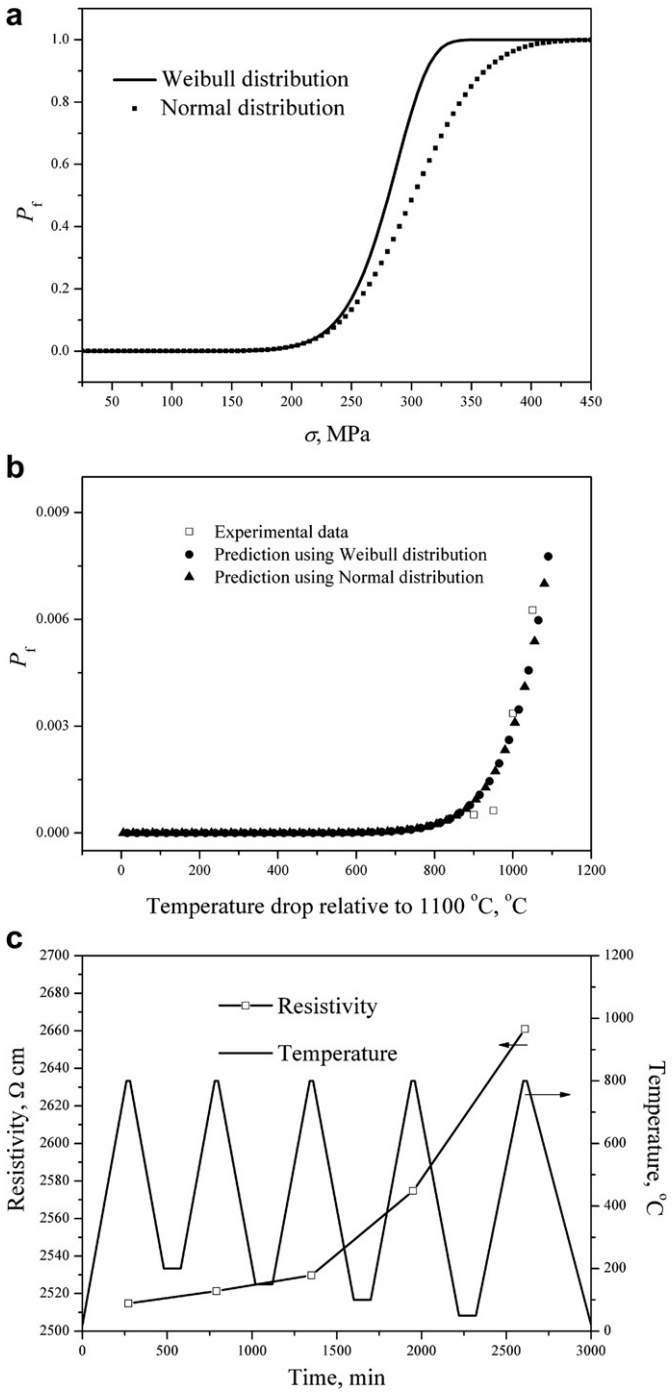

Fig. 8. (a) Weibull distribution with $\sum = 208$ MPa and $m = 11.4$ and normal distribution with $\bar{\sigma} = 302$ MPa and $\delta = 46.5$; (b) ΔT–P_f curve derived from the σ–P_f curve shown in Fig. 8a. The composite contains 25 wt.% Al_2O_3. The experimental results obtained at different ΔT from Fig. 8c are also shown for comparison; (c) Resistivity at 800 °C for an YSZ–Al_2O_3 (75:25) composite undergoing thermal cycles in different temperature ranges.

and the increment of each cycle is bigger for a higher ΔT. Through calculation of the average coordination number using Eqs. (5)–(7) at different thermal cycle stage, the failure probability between YSZ particles is obtained. The results are also shown in Fig. 8b. The experiment data agrees well with the model prediction derived from the Weibull distribution with $\sum = 290$ MPa and $m = 11.4$ as well as the normal distribution with $\bar{\sigma} = 302$ MPa and $\delta = 46.5$. So, this method can predict the fracture situation of composites enduring thermal cycles in any temperature ranges.

5. Conclusion

A novel method is presented to detect the relationship between the particle–particle fracture of YSZ in the YSZ–Al_2O_3 composites and the conductivity combining the Weibull or normal distribution, the percolation theory and a simple approach to calculate the thermal stress in thermal cycle processes. When YSZ is sintered at 1100 °C, the results are that $\sum = 290$ MPa and $m = 11.4$ for the Weibull distribution as well as $\bar{\sigma} = 302$ MPa and $\delta = 46.5$ for the normal distribution. Thus, the cracking between particles can be determined. Accordingly, the influence of the cracking on resistivity can be precisely predicted. This method provides a new methodology to well understand the mechanical behaviors between particles and to approach the parameters through numerous fractures. In addition, this method makes it feasible to precisely predict the structural failure of the composite electrodes in SOFCs and performance attenuation under harsh conditions such as thermal cycle.

Acknowledgements

We gratefully acknowledge the Ministry of Science and Technology of China (2012CB215403).

References

[1] L. Yang, S.Z. Wang, K. Blinn, M.F. Liu, Z. Liu, Z. Cheng, M.L. Liu, Science 326 (2009) 126–129.
[2] C.R. Xia, M.L. Liu, Adv. Mater. 14 (2002) 521–523.
[3] S.B. Adler, Chem. Rev. 104 (2004) 4791–4843.
[4] A. Atkinson, B. Sun, Mater. Sci. Technol. 23 (2007) 1135–1143.
[5] W. Bujalski, C.M. Dikwal, K. Kendall, J. Power Sources 171 (2007) 96–100.
[6] S. Taniguchi, M. Kadowaki, T. Yasuo, Y. Akiyama, Y. Miyake, K. Nishio, J. Power Sources 90 (2000) 163–169.
[7] H. Yakabe, Y. Baba, T. Sakurai, M. Satoh, I. Hirosawa, Y. Yoda, J. Power Sources 131 (2004) 278–284.
[8] C.S. Montross, H. Yokokawa, M. Dokiya, Br. Ceram. Trans. 101 (2002) 85–93.
[9] A. Selimovic, M. Kemm, T. Torisson, M. Assadi, J. Power Sources 145 (2005) 463–469.
[10] A. Atkinson, A. Selcuk, Solid State Ionics 134 (2000) 59–66.
[11] L. Liu, G.-Y. Kim, A. Chandra, J. Power Sources 195 (2010) 2310–2318.
[12] F. Zhao, R.R. Peng, C.R. Xia, Mater. Res. Bull. 43 (2008) 370–376.
[13] A. Nakajo, Z. Wuillemin, J. Van herle, D. Favrat, J. Power Sources 193 (2009) 216–226.
[14] D.F. Chen, Z.J. Lin, H.Y. Zhu, R.J. Kee, J. Power Sources 191 (2009) 240–252.
[15] P. Costamagna, P. Costaand, V. Antonucci, Electrochim. Acta 43 (1988) 375–394.
[16] Y.X. Zhang, C.R. Xia, J. Power Sources 195 (2010) 6611–6618.
[17] R.W. Rice, J. Mater. Sci. 40 (2005) 983–989.
[18] A. Nakajo, C. Stiller, G. Harkegard, O. Bolland, J. Power Sources 158 (2006) 287–294.
[19] M. Mori, Y. Abe, H. Itoh, O. Yamamoto, Y. Takeda, T. Kawahara, Solid State Ionics 74 (1994) 157–164.
[20] Chawla, K. Kumar, Ceramic Matrix Composites, Kluwer Academic Publishers, Boston, 2003.
[21] J. Sanyal, G.M. Goldin, H.Y. Zhu, R.J. Kee, J. Power Sources 195 (2010) 6671–6679.
[22] C.-H. Kuo, P.K. Gupta, Acta Metall. Mater. 43 (1995) 397–403.
[23] J.W. Fergus, J. Power Sources 162 (2006) 30–40.
[24] A. De, S. Jayatilaka, K. Trustrum, J. Mater. Sci. 12 (1977) 1426–1430.
[25] C.S. Lu, R. Danzer, F.D. Fischer, Phys. Rev. E 65 (2002) 067102.